

Comparison of Location Procedures: The Kara Sea Event of 16 August 1997

by Johannes Schweitzer and Brian L. N. Kennett

Abstract Various location procedures and velocity models are compared for the M_L 3.3 Kara Sea event of 16 August 1997. This event has been the subject of considerable discussion because of its geographical position and the difficulty in obtaining a reliable focal-depth estimate. A comprehensive data set was extracted by (re-)reading the records from all available stations. These readings have then been used in a sequence of location experiments to examine the effect of using different velocity models to describe the travel times of the phases, and also to compare the use of a fully nonlinear scheme (shakeNA; Sambridge and Kennett, 2001) and a linearized location algorithm (HYPOSAT; Schweitzer, 2001, 2002). A standard least-squares misfit criterion has been used for direct comparisons between the two methods.

The results confirm both the importance of *S*-wave information in assessing the depth of regional events, and the need to apply a reliable velocity model to place the strongest constraints on the location of the event. Even with only a limited data set, but an adequate velocity model, it is possible to find the position of the Kara Sea event close to the most probable locations; however, there is then no depth resolution. Reported error ellipses from standard data centers tend to have relatively small error ellipses. With the commonly made assumption that the reading errors and the *a posteriori* residuals have an unbiased normal distribution, such inversion results may indicate an unreasonably high resolution and accuracy of the solution.

The epicenter estimates for the whole data set using the range of different techniques agree quite well, with some overlap of the estimated confidence regions. The observed seismic source was most likely an earthquake in the middle or lower crust at about 10–30 km depth.

Introduction

A seismic event in the Kara Sea region to the east of Novaya Zemlya on 16 August 1997 at about 02:11 UT has been the subject of considerable discussion (e.g., Hartse, 1998; Bowers, 2002) because of its geographical location near the former nuclear test site of the former Soviet Union. All published estimates of the epicenter locate the event in the Kara Sea. However, the very limited set of station readings available in the bulletins of the International Seismological Centre (ISC) and of the Prototype International Data Center (PIDC) is not adequate to constrain the depth effectively. Could this M_L 3.3 event (Hicks *et al.*, 2004) have been an underwater explosion?

A more comprehensive data set has been assembled by (re-)picking all available records from this event, including the closest station AMD at the northern end of the Urals at about 320 km range. The distribution of seismic stations, for which readings have been made, is shown in Figure 1, the corresponding station coordinates are listed in Table 1, and

the full-phase list with arrival time, slowness, and azimuth readings is presented in Table 2.

Many of the stations lie in Fennoscandia, but azimuthal control is improved by some observations in the western Barents Sea and in Russia. The total data set contains many *S*-phase readings. Some of the *S* times have significant reading uncertainties (see Table 2), but they all can help to provide control on position and depth through the sensitivity of the differential *S*-*P* times to distance.

A sequence of location experiments have been undertaken to compare the results of using both different velocity models to describe the travel times of the phases and two different location programs, a linearized location algorithm (HYPOSAT; Schweitzer, 2001, 2002b) and a fully nonlinear scheme (shakeNA; Sambridge and Kennett, 2001). For direct comparisons between the two methods, we have used a standard least-squares misfit criterion, but have also examined the influence of more robust choices for data misfit

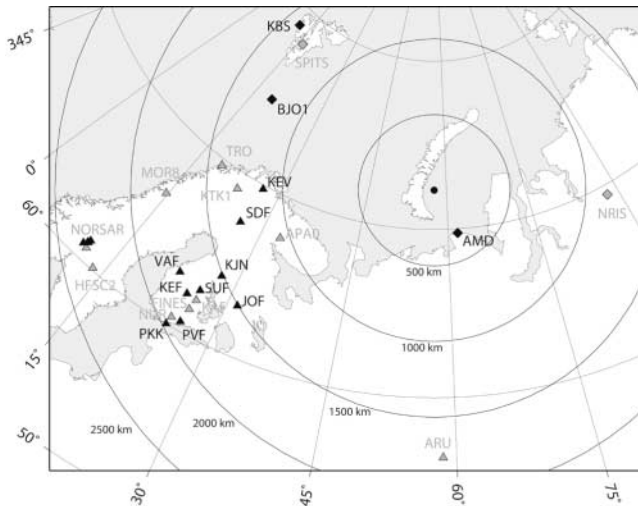


Figure 1. Seismic stations (triangles and diamonds) that recorded the seismic event in the Kara Sea on 16 August 1997 (black dot). Triangles and diamonds were used for stations for which the models BAREY and BAREZ, respectively, gave the best results when calculating travel times for the joint model COMB. The gray symbols show stations that contributed with observed onset data to the bulletins of the international data centers, and the black symbols represent stations with additionally analyzed data (this study). The circles show distances from the event in steps of 500 km.

when using the nonlinear location scheme. Finally, we compare our solutions with published results of international data centers.

Tested Velocity Models and Observed Data

To locate the Kara Sea event, the global reference models JB (Jeffreys and Bullen, 1940), PREM (Dziewonski and Anderson, 1981), IASP91 (Kennett and Engdahl, 1991), and AK135 (Kennett *et al.*, 1995) have been used, and we have also considered two regional models derived from the BARENTS model of Kremenetskaya *et al.* (2001). These three regional models are shown in Figure 2. Both new regional models have identical P velocities, which had to be changed slightly with respect to the BARENTS model to achieve a numerical stable application of this model to the tau-spline-based travel-time-table software (Buland and Chapman, 1983) implemented in the location routines. The corresponding S velocities were constructed by two different approaches:

- A P -to- S velocity ratio (V_P/V_S) of 1.73 is used by NORARSAR (Mykkeltveit and Ringdal, 1981) in its standard velocity model to locate seismic events in Fennoscandia and its surrounding areas. We applied this velocity ratio to the regional P -velocity model and named the model BAREZ, which uses a V_P/V_S ratio of 1.73 in the crust and the ratio 1.72 below the Moho.

- Using Wadati's method (Wadati, 1933), one can obtain an estimate of the source time and the V_P/V_S ratio from S - P travel-time differences. At 13 stations not only the first P but also the first S onsets were readable. Since all these observation pairs belong to P_n and S_n onsets at a distance range from about 3 to 16°, the corresponding V_P/V_S ratio represents the V_P/V_S ratio below the Mohorovičić discontinuity in the uppermost mantle. The mean observed V_P/V_S ratio is 1.779 ± 0.006 , which is close to the ratio in the original BARENTS model, but somewhat higher than in the BAREZ model. Therefore, we decided to introduce a second model closer to this observed velocity ratio by lowering the V_P/V_S ratio in the uppermost mantle to 1.770 in the model BAREY.

During our location tests, we have found that the BAREY model is appropriate for the onset times along paths from the Kara Sea to Fennoscandia, but that the BAREZ model is more suitable for paths from the Kara Sea to Spitsbergen, Bear Island, and Northern Siberia. This finding agrees well with the fact that the travel paths of the observed seismic waves are dominated by two principal crustal units: either the continental shelf of the European Arctic or the Fennoscandian shield (Mooney *et al.*, 1998). Although both models are relatively simple approximations of an area known to be laterally heterogeneous (e.g., Levshin *et al.*, 2001; Bungum *et al.*, 2005), a recent study showed that the BAREY model is suitable for event location in the whole European Arctic for observations at stations in and around Fennoscandia (Hicks *et al.*, 2004).

The source time calculated with Wadati's method is $02:11:06.6 \pm 0.4$. The correct source time has to be slightly earlier because inverting S_n - P_n differential times cannot model the requisite velocity ratio on the relatively short travel paths through the crust. However, such travel paths will not change the calculated V_P/V_S ratio significantly, because only a small constant is added to the S_n - P_n travel-time differences, which will only be slightly changed by different crustal structures below the stations.

All the observations listed in Table 2 were uniformly and carefully investigated and evaluated during this study. The onset times were determined by using an autoregressive picking algorithm on the digital records (Akaike, 1974; Group of Scientific Experts [GSE], 1992), which is implemented in the NORARSAR analysis software (ARAIC; compare Kværna, 1995). This algorithm also gives information on the uncertainty of the onset-time reading by the width and form of the minimum of the AIC trace (Kværna, 1995). This uncertainty was used as the standard observation error in our inversions. To exploit the widest possible frequency range of the recorded signals, the records were Butterworth band-pass filtered to just remove the most prominent microseismic noise before applying the ARAIC algorithm. Slowness vectors could also be measured for all P and S onsets observed by seismic arrays (see Table 2). However, their contribution

Table 1
Stations Used in This Study and Their Coordinates (see also Fig. 1)

Station Code – Name	Latitude (°)	Longitude (°)	Elevation (m)	PIDC	NEIC	ISC	This Study
AMD – Amderma, Russia	69.7420	61.6550	200.0	—	—	—	*
APA0 – Apatity array, beam reference point, Russia	67.6033	32.9944	200.0	—	—	*	*
ARU – Arti, Russia	56.4302	58.5625	250.0	*	—	*	—
BJO1 – Bjørnøya (Bear Island)	74.5020	18.9990	18.0	—	—	—	*
FINES – FINES array, beam reference point, Finland	61.4439	26.0738	150.0	*	*	*	*
HFSC2 – Hagfors array, beam reference point, Sweden	60.1326	13.6958	265.0	*	*	*	*
JOF – Joensuu, Finland	62.9182	31.3124	180.0	—	—	—	*
KAF – Kangasniemi, Finland	62.1112	26.3061	195.0	—	*	*	*
KBS – Ny Ålesund (Kingsbay), Svalbard Archipelago	78.9168	11.9173	46.0	—	—	—	*
KEF – Keuruu, Finland	62.1664	24.8706	215.0	—	—	—	*
KEV – Kevo, Finland	69.7553	27.0067	81.0	—	—	—	*
KJN – Kajaani, Finland	64.0857	27.7110	262.0	—	—	—	*
KTK1 – Kautokeino, Norway	69.0115	23.2354	340.0	—	—	*	*
MOR8 – Mo i Rana, Norway	66.2855	14.7352	445.0	—	—	*	*
NAO01 – NORSAR array, three-component site, Norway	60.8442	10.8865	426.0	—	—	—	*
NB201 – NORSAR array, three-component site, Norway	61.0495	11.2939	613.0	—	—	—	*
NB2 – NORSAR array, beam reference point, Norway	61.0397	11.2148	717.0	—	—	*	—
NC303 – NORSAR array, three-component site, Norway	61.2251	11.3690	401.0	—	—	—	*
NC602 – NORSAR array, three-component site, Norway	60.7353	11.5414	305.0	—	—	—	*
NORES – NORES array, beam reference point, Norway	60.7353	11.5414	302.0	*	*	*	*
NRIS – Noril'sk, Russia	69.0061	87.9964	498.0	*	*	*	*
NUR – Nurmijarvi, Finland	60.5090	24.6510	102.0	—	*	*	*
PKK – Porkkala, Finland	60.0052	24.5169	10.0	—	—	—	*
PVF – Pernaja, Finland	60.5451	25.8616	45.0	—	—	—	*
SDF – Sodankyla, Finland	67.4203	26.3936	276.5	—	—	—	*
SPITS – Spitsbergen array, beam reference point, Svalbard Archipelago	78.1777	16.3699	323.0	*	*	*	*
SUF – Sumiainen, Finland	62.7191	26.1506	185.0	—	—	—	*
TRO – Tromsø, Norway	69.6345	18.9077	15.0	—	—	*	*
VAF – Ylistaro, Finland	63.0422	22.6715	55.0	—	—	—	*

An asterisk indicates if the reading(s) of this station were used either by international agencies or in this study.

to the final location accuracy is negligible, because they show low sensitivity to small hypocentral changes.

The final inversions were made without including some of the available data. The *S* onsets at KTK1 and TRO were not used because the triggered data contain only the last part of the seismograms and not the *P* onsets; the *P* onset at MOR8 was not used because we suspected an absolute timing error at this station. The ISC used a reported onset for NB2, which is the code used by NORSAR when reporting an onset on the short-period beam calculated for the whole NORSAR array. Instead of recalculating this beam, we analyzed the onsets for all available three-component broadband traces (NAO01, NB201, NC303, and NC602) of the NORSAR array. NC602 is collocated with the center element (NRA0) of the NORES array, and to avoid duplication we dropped the NC602 reading in our final analyses. In the Reviewed Event Bulletin (REB) of the PIDC, an *Sn*-onset time for station ARU is included. We requested the ARU data from the PIDC to reanalyze these records. After carefully checking the three-component data around the presumed and reported onset time, we could not confirm any *Sn* onset from the expected backazimuth and rejected this reading. This spurious onset is also listed in the ISC bulletin, but was never used as constraining observation at the PIDC or at the ISC. Thus, our final inversion employs 23 *P*-phase and 13 *S*-phase

readings from 23 different seismic stations covering a distance range of about 3 to 21° (330 to 2400 km).

Location Results with the Neighborhood Algorithm shakeNA

The nonlinear location procedure shakeNA using the Neighborhood Algorithm (NA) is based on an exploration of the four-dimensional hypocentral parameter space to find models with good fit to the data (Sambridge and Kennett, 2001). At each stage, the algorithm makes use of all the information from prior sampling to define a partition of the parameter space into Voronoi cells around each sampled point describing the region that lies closest to that point. To find effective location estimates the algorithm is used in a fairly focused way with an initial sampling of nine points in the entire specified volume and then nine new points in each iteration randomly sampling the current two “best” Voronoi cells, that is, those containing the points with the least misfit. In this mode, the progress of the nonlinear inversion resembles the convergence of a cloud of points towards a single-location estimate. Because no derivatives are required it is possible to employ any convenient measure of data fit, in particular, an $L_{1.25}$ norm (cf. Billings *et al.*, 1994) provides a convenient compromise between robustness and fidelity to

Table 2
Onset Times, Backazimuth Values (BAZ), and Ray Parameters (P) and Their Standard Deviations σ for the First P- and S-Type Onsets Derived from Rereading Seismograms

Station	Δ (°)	AZI (°)	Phase	Hour	Minute	Second	σ Time (sec)	BAZ (°)	σ BAZ (°)	P (sec/°)	σ P (sec/°)	Remarks
AMD	2.917	151.1	P	02	11	48.50	0.10	—	—	—	—	I-2
AMD	2.917	151.1	S	02	12	21.15	0.20	—	—	—	—	I-2
APA0	9.623	252.7	P	02	13	17.14	1.50	72.7	25.0	9.03	4.0	I-C
APA0	9.623	252.7	S	02	15	02.84	2.00	53.5	25.0	19.24	4.0	I-C
BJO1	11.091	299.3	P	02	13	35.98	3.00	—	—	—	—	I-2
BJO1	11.091	299.3	S	02	15	30.60	5.00	—	—	—	—	I-2
FINES	16.226	244.1	P	02	14	46.33	1.75	33.2	15.0	10.90	1.5	I-C
FINES	16.226	244.1	S	02	17	37.83	3.00	—	—	—	—	I-C
HFSC2	20.856	257.2	P	02	15	42.82	0.50	28.0	15.0	9.42	2.0	I-C
JOF	16.604	239.6	P	02	14	09.86	1.00	—	—	—	—	I
JOF	16.604	239.6	S	02	16	33.42	2.00	—	—	—	—	I
KAF	15.616	245.2	P	02	14	36.00	2.00	—	—	—	—	I-C
KBS	12.707	321.0	P	02	13	57.47	1.00	—	—	—	—	I-2
KBS	12.707	321.0	S	02	16	08.06	2.00	—	—	—	—	I-2
KEF	15.973	247.3	P	02	14	42.72	0.75	—	—	—	—	I
KEV	10.207	270.3	P	02	13	25.19	0.50	—	—	—	—	I
KEV	10.207	270.3	S	02	15	13.18	2.50	—	—	—	—	I
KJN	13.663	248.0	P	02	14	12.32	2.00	—	—	—	—	I
KJN	13.663	248.0	S	02	16	39.60	2.00	—	—	—	—	I
KTK1	11.737	270.5	S	02	15	50.37	2.50	—	—	—	—	C
MOR8	15.974	269.4	P	02	14	41.42	1.50	—	—	—	—	C
NAO01	21.131	261.5	P	02	15	45.44	0.60	—	—	—	—	I
NB201	20.846	261.4	P	02	15	43.07	0.60	—	—	—	—	I-C
NC303	20.686	261.6	P	02	15	41.27	0.50	—	—	—	—	I
NC602	21.019	260.6	P	02	15	44.57	0.50	—	—	—	—	—
NORES	21.019	260.6	P	02	15	44.55	0.50	37.1	15.0	10.08	1.2	I-C
NRIS	10.523	93.5	P	02	13	30.19	1.00	—	—	—	—	I-2-C
NRIS	10.523	93.5	S	02	15	19.35	1.50	—	—	—	—	I-2-C
NUR	17.392	244.2	P	02	15	02.00	2.00	—	—	—	—	I-C
PKK	17.851	243.5	P	02	15	07.90	1.50	—	—	—	—	I
PVF	17.031	242.6	P	02	14	58.18	1.50	—	—	—	—	I
SDF	11.701	260.7	P	02	13	45.17	1.00	—	—	—	—	I
SDF	11.701	260.7	S	02	15	50.75	2.00	—	—	—	—	I
SPITS	11.730	318.0	P	02	13	44.85	0.50	103.0	15.0	11.98	2.5	I-2-C
SPITS	11.730	318.0	S	02	15	45.45	1.50	95.0	15.0	19.86	2.5	I-2-C
SUF	15.172	246.8	P	02	14	31.29	1.00	—	—	—	—	I
SUF	15.172	246.8	S	02	17	13.10	3.00	—	—	—	—	I
TRO	12.734	276.8	S	02	16	15.40	2.50	—	—	—	—	C
VAF	15.913	252.2	S	02	17	29.83	2.00	—	—	—	—	I
VAF	15.913	252.2	P	02	14	41.05	1.50	—	—	—	—	I

Epical distances (Δ) and station azimuths (AZI) were calculated with respect to the COMB solution of Table 3. To find this and all other solutions of this table, all data marked with an “I” were used in the inversions. For the COMB solutions, we used model BAREY for all onset-time observations except for those indicated with a “2,” for which model BAREZ was applied. A “C” marks data used in the comparisons with solutions published by international data centers (see Table 4).

observations. For comparison with the HYPOSAT scheme an L_2 norm is used in the illustrated inversions.

The NA scheme was applied to a zone 16° across in longitude and 8° across in latitude and extending to 120 km deep, centered in the Kara Sea, and up to 20 sec variation in origin time was also allowed. Despite the large initial domain, convergence is rapid and low misfits can readily be achieved in about 30 iterations. The misfit level for the two global reference models AK135 and IASP91 is comparable, but AK135 provides a slightly better fit. A variance reduction of about 30% compared with the global models can be achieved by using the region-specific models, BAREY and BAREZ.

In Figure 3, we show the central portion of the parameter space (a 20-km square around a reference point) for the BAREZ model with a conventional least-squares (L_2) misfit measure. The NA algorithm has been extended here to 60 iterations to provide a further exploration of the zone of better misfit. The group of black models has a very similar misfit and defines a “consistency region” marked with a shaded polygon, which indicates the variability allowed in the event location.

This consistency region is defined with the aid of an auxiliary weighting function, based on analogs from statistical physics (Kennett, 2004). The threshold in the auxiliary function can be translated into an equivalent upper limit to

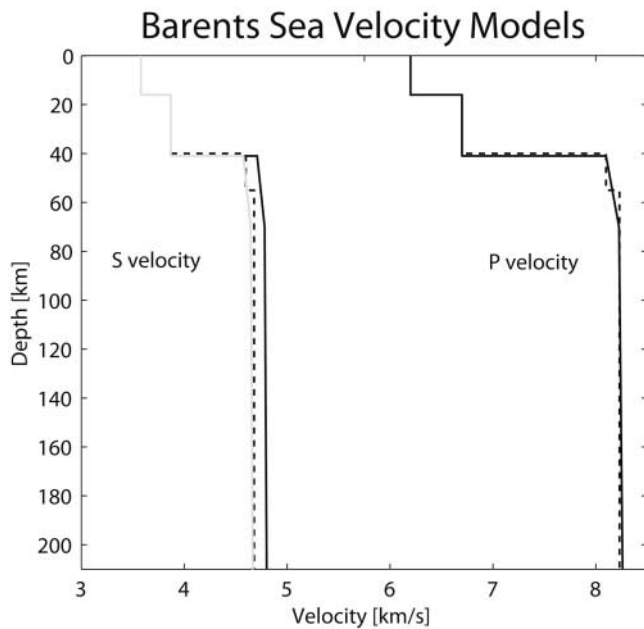


Figure 2. Plot of regional velocity models used in this study. The models BAREY (gray line) and BAREZ (black lines) were both derived from the BARENTS model (dotted lines, from Kremenetskaya *et al.*, 2001). Note that the P velocities in the models BAREY and BAREZ are identical.

the value of the misfit function. For an L_2 norm, the consistency region is chosen to be such that the misfit level is equivalent to that employed for the error ellipsoid from HYPOSAT, but there is no restriction to ellipsoidal shape (via a local quadratic assumption). The polygonal region encloses the acceptable samples in the four-dimensional hypocentral space. The consistency-region approach can also be used directly with other measures of misfit to outline the domain of suitable solutions.

It is easier to derive a threshold scheme for the weighting function than for the misfit itself, because the shape of the weighting function is known and only the scaling varies. Only a marginal difference exists between the levels of misfit for the solutions indicated with black symbols. The solution with best fit to data is indicated with the open diamond, but a more useful quantity is generally the ensemble-weighted average indicated with the grey cross in Figure 3.

The exploratory nature of the NA algorithm allows alternative regions of good fit with a different combination of depth and origin time to be found. The sensitivity of the data misfit varies over different zones of the hypocenter space, and indeed groups of location estimates with very similar levels of misfit can exist. This is illustrated with Figure 4, where we show the central portion of the parameter space for model IASP91; subregions of equally good misfit levels can clearly be identified, notably in depth.

The epicentral areas of all four models tested with the NA algorithm are plotted in Figure 5; Table 3 lists the corresponding numerical results. The polygons in each case rep-

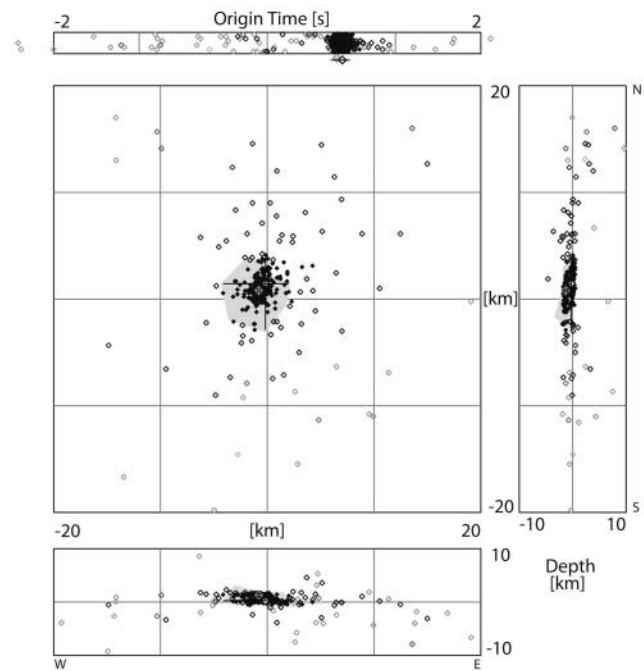


Figure 3. A zoom view of the four-dimensional hypocenter space searched with the shakeNA algorithm applying an L_2 norm scheme, shown as a map view and depth slices around the portion of the sampled region centered on a reference point at 72.40° N, 57.90° E, 20.0 km depth, and 2.0 sec origin time. The different panels show the four-dimensional hypocentral solution space for an area of ± 20 km around the epicentral reference point, ± 10 km around the reference depth, and ± 2 sec around the reference origin time. The progress of the direct method toward a location estimate for the regional BAREZ model is indicated by projecting the successive hypocenter estimates onto the sections, with a coding by misfit that becomes darker as the misfit in the arrival times is reduced. The region of acceptable misfits is indicated with black filled symbols. The estimate of the consistency region in four-dimensional hypocenter space associated with these acceptable models is indicated with gray shading. The region of acceptable misfits is indicated with black filled symbols. The estimate of the consistency region in four-dimensional hypocenter space associated with these acceptable models is indicated with gray shading. The ensemble properties indicated by the gray polygon and cross give a good indication of the location and its uncertainties.

resent the consistency region of the solution for the velocity model employed. In addition, we have plotted two solutions: the location with the minimum misfit as an open, black symbol and the mean of the whole ensemble of solutions defining the consistency region as a filled, gray symbol. The shakeNA locations for the standard Earth models IASP91 and AK135 are very close and clearly separated by 15–20 km from the solutions using the regional models BAREY and BAREZ, which show somewhat smaller consistency regions.

All shakeNA hypocenter estimations with small residuals give depths in the lower crust. The less appropriate global models IASP91 and AK135 give depths in the lowermost crust between 30 and 40 km, and for the regional models BAREY and BAREZ depths were found between 18 and 30 km.

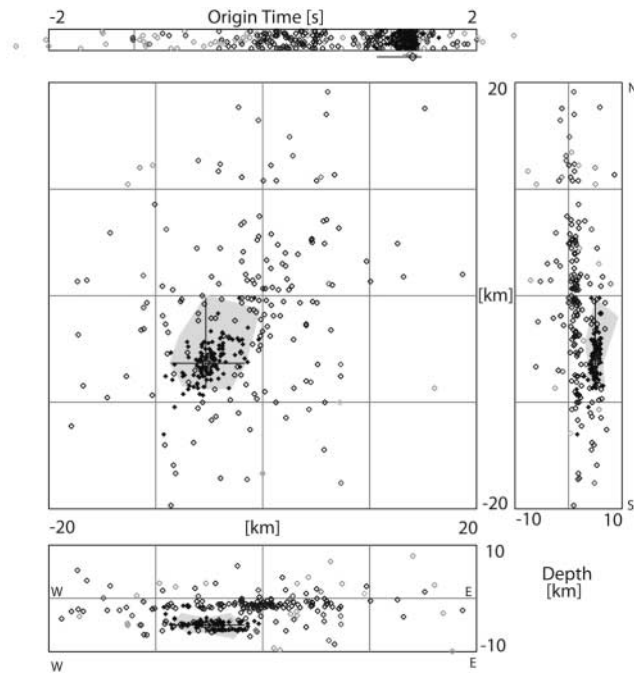


Figure 4. Similar zoom view of the shakeNA results for the model IASP91, the reference point is displaced to 72.40° N, 57.50° E, 30.0 km depth, and 2.0 sec origin time to accommodate the shift in the position of best fit for this global model. In the depth sections we can clearly see two groups of models at different depths with similar levels of misfit, indicating the presence of pronounced local minima in the misfit.

For a quantitative measure of the quality of an event location, we have calculated two different parameters: the root-mean-square (rms) of all constraining onset times and a weighted mean misfit of all observations (travel times, backazimuth values, and ray parameters) used in the last iteration of the inversion (WMF). The WMF is defined by calculating the mean of all residuals weighted by their standard deviations, respectively. The rms and WMF are also listed for each hypocenter determination in Table 3.

The presence of sets of solutions with very similar levels of fit poses problems when using a linearized inverse scheme, for example, HYPOSAT. Such an algorithm will tend to be pulled toward one particular epicentral subregion or depth range (e.g., depending on where it was initiated), and unlike the nonlinear scheme it will not be able to escape to find a better point. Varying the initial solution may help in some cases but does not guarantee that the global minimum is always found. If we are unlucky, it is possible that the sequence of location estimates will approach the minimum from a direction such that the estimated model parameter changes of this iteration overshoot the minimum and that at the subsequent iteration the changes return to or near the earlier point. Such oscillations are difficult to tame.

In both the nonlinear and linearized inversions, we found that the patterns of residuals when using either the BAREY or the BAREZ model reveal an inconsistency be-

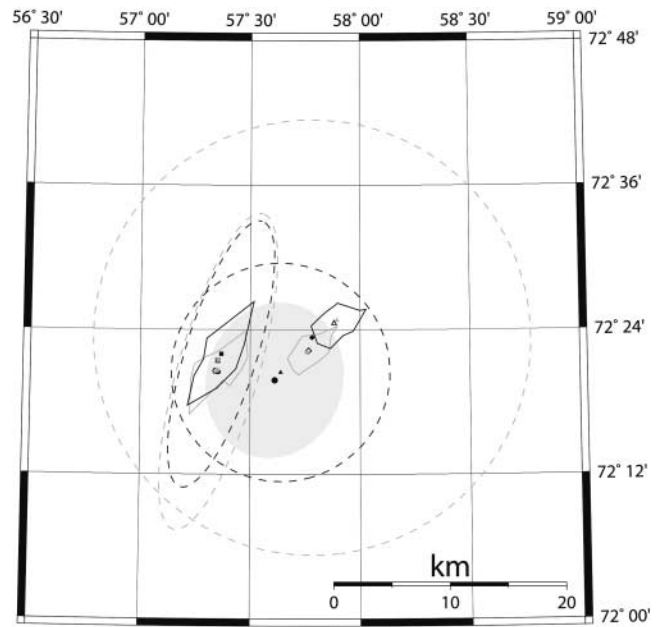


Figure 5. Inversion results for shakeNA (polygons, full lines) and HYPOSAT (error ellipses, dashed lines) for the full data set and the different velocity models IASP91 (black hexagons, gray uncertainty areas), AK135 (squares, black uncertainty areas), BAREZ (triangles, black uncertainty areas), BAREY (diamonds, gray uncertainty areas), and COMB (black dot, gray-shaded uncertainty area). For further details, see text and Table 3.

tween *S* waves on paths to Spitsbergen and Siberia compared with those to Fennoscandia. One group of arrivals or the other group is well fitted, but always with significant residuals for the second group (see also Fig. 6). This suggests that different models should be employed for the two sets of travel paths.

Comparison with the HYPOSAT Results

HYPOSAT (Schweitzer, 2001, 2002b) is based on a linearized inversion scheme and has additional features compared with the shakeNA algorithm; it has the potential of utilizing ray parameter-dependent altitude corrections, travel-time differences between phases, and combining different velocity models for different ray paths. All input data are normalized by their observed standard deviations and the program recalculates all partial derivatives before each iteration of the generalized matrix inversion (e.g., Menke, 1989). The inverted matrix is calculated by applying the singular-value decomposition algorithm as published in Press *et al.* (1992). An analysis of the information density matrix (e.g., Menke, 1989) shows that this algorithm automatically reduces the influence of redundant information on the modeled parameters. However, for direct comparisons with the shakeNA results, the HYPOSAT inversions were restricted to a strict least-squares scheme. All error ellipses for the

Table 3
The New Hypocenter Solutions for the 16 August 1997 Kara Sea Event as Plotted in Figure 5

Model	Latitude (°)	Longitude (°)	<i>D</i> (km)	σ or Range for <i>D</i> (km)	Time	OT (36)	BAZ (7)	RP (7)	WMF (36)	rms (sec)	EE (km ²)	M
AK135	72.357	57.352	35.1	31.4–36.3	02:11:03.38	36	7	7	2.65	4.64	—	NA-B
AK135	72.358	57.354	34.8	31.4–36.3	02:11:03.35	36	7	7	2.65	4.66	—	NA-M
AK135	72.366	57.367	34.4 F	13.2–51.8	02:11:00.42	36	7	4	3.65	3.69	368	H
IASP91	72.343	57.342	35.0	32.3–36.5	02:11:03.40	36	7	7	2.86	5.08	—	NA-B
IASP91	72.344	57.350	34.9	32.3–36.5	02:11:03.38	36	7	7	2.87	5.07	—	NA-M
IASP91	72.342	57.354	36.9 F	11.3–61.6	02:11:03.46	36	6	3	3.99	4.06	491	H
BAREY	72.371	57.765	29.2	24.5–30.1	02:11:03.61	36	7	7	1.27	1.98	—	NA-B
BAREY	72.369	57.758	27.7	24.5–30.1	02:11:03.44	36	7	7	1.27	1.98	—	NA-M
BAREY	72.389	57.781	38.2	10.3	02:11:04.09	32	4	1	1.22	1.20	3528	H
BAREZ	72.413	57.895	19.7	18.2–20.5	02:11:02.70	36	7	7	1.59	3.59	—	NA-B
BAREZ	72.409	57.882	19.1	18.2–20.5	02:11:02.67	36	7	7	1.58	3.59	—	NA-M
BAREZ	72.341	57.638	15.9	7.5	02:11:02.85	29	4	1	1.55	1.34	884	H
COMB	72.330	57.611	17.6	5.2	02:11:02.91	36	5	1	0.91	1.27	396	H

The source parameters are presented together with the number of onset times (OT), backazimuth values (BAZ), and ray parameters (RP) used by HYPOSAT as constraining observations. In the header line, the maximum possible number for each of these input data is given in parentheses. WMF is the weighted mean misfit for all available travel-time observations and root-mean-square (rms) was calculated from all constraining onset times. An “F” together with the estimated depth indicates that the depth was fixed by the program. EE lists the size of the error ellipse as plotted in Figure 5. “M” indicates the location algorithm used. NA-B, the shakeNA solution with the smallest misfit; NA-M, the mean of all shakeNA solutions in the consistency region; and H, the HYPOSAT solution.

epicenters were calculated for a 90% significance level after projecting the corresponding uncertainties of source time and event depth in consideration of the covariance matrix into the epicentral-error space. The iteration process was stopped whenever the hypocentral distance between two sequential solutions was less than 0.5 km. To force a stable result, the program itself removes some observations during the iterations of the inversion if the residuals became too large. Therefore, the number of constraining input data changes slightly between the different solutions.

As for the shakeNA scheme, the two standard Earth models IASP91 and AK135 and the two regional models BAREZ and BAREY were used for locating the Kara Sea event with HYPOSAT. The corresponding epicenters are plotted together with the shakeNA results in Figure 5 and they are also presented in Table 3. The HYPOSAT epicenters are plotted with filled symbols and their corresponding error ellipses appear as dashed lines. The error ellipses and epicenters for the standard Earth models IASP91 and AK135 are in close accord with the shakeNA results. However, because of the limitations of these velocity models at regional distances, the inversions for both models oscillated between a source depth in the middle crust and below the Mohorovičić discontinuity. It was therefore necessary for the program to fix the depth of the event. The result of this reduction in source parameters is a reduction of the dimension of the covariance matrix, and consequently, we find relatively small error ellipses, although the rms and WMF values are relatively large.

The phase times are sufficiently consistent with models BAREZ and BAREY that HYPOSAT was also able to invert for the depth of the event. As in shakeNA, both models can only directly explain a subset of data, depending on the ac-

tual ray paths. For BAREY the *S*-phase observations on Spitsbergen and on Bear Island could not be modeled very well and were declared as nonconstraining observations during the inversion. The estimated hypocenter itself is similar to the shakeNA result. However, for model BAREY the error ellipse is very large because of the large depth error of ± 10.3 km, which is projected on the epicentral uncertainty. For BAREZ all residuals of the *S* observations in Fennoscandia became very large and were refused as constraining input data. Consequently, the set of input data became more homogeneous but the error ellipse is still relatively large, mostly because of the depth error of about ± 7.5 km. The agreement with the shakeNA solutions for BAREZ is worse, but most of the shakeNA consistency region and all shakeNA solutions lay within the error ellipse of the HYPOSAT solution.

The data set for this Kara Sea event shows a non-Gaussian distribution in observed travel-time residuals, as shown in the histograms of the final travel-time residuals in Figure 6 of all available onset times. The distribution of residuals is independent of the location algorithms, here shown for model BAREY. From Figure 6 it also becomes obvious that the global velocity models IASP91 and AK135 are not really suitable for locating this event. To account for the non-Gaussian character of the travel-time residuals, the original HYPOSAT code was extended to apply different travel-time tables after choosing the best travel-time table for each path (see Table 2). For the final solution, here called COMB (Fig. 5, dot with gray-shaded error ellipse), we applied all possibilities of HYPOSAT (i.e., correcting station elevations, inverting for travel-time differences between the different phase onsets at one station and choosing the travel-time table with respect to the paths as indicated in Table 2). The result of this inversion is a hypocenter solution with a

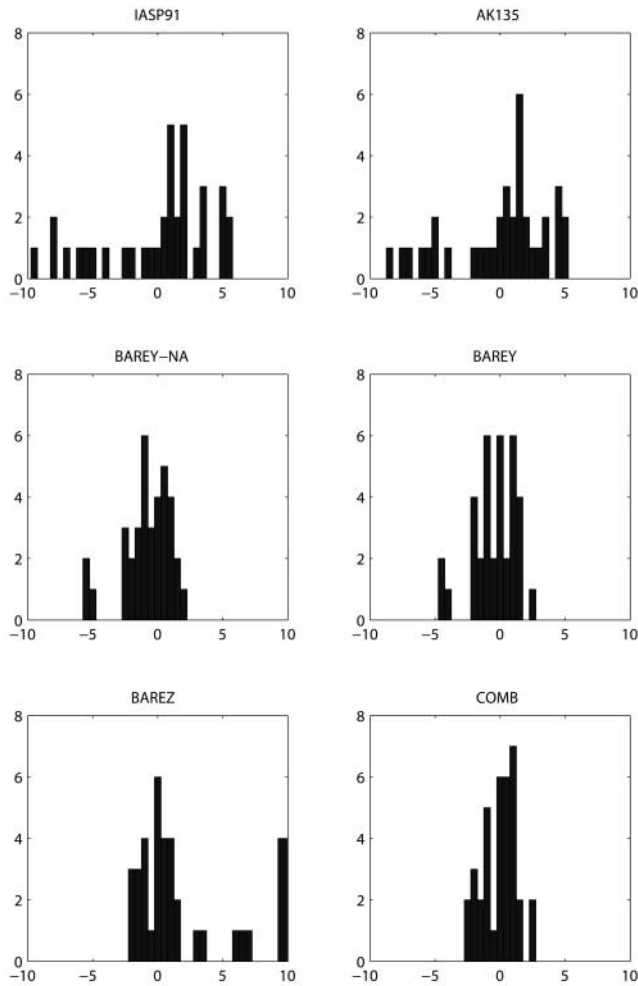


Figure 6. Histogram of all travel-time residuals (i.e., for all constraining and nonconstraining onset times) in seconds after locating the event with different velocity models using in all cases HYPOSAT as the location routine, except for BAREY-NA, which shows the shakeNA results (see also Fig. 5 and Table 3).

smaller horizontal error ellipse, very small data residuals, and an inverted (i.e., not fixed) depth with an estimated uncertainty of only ± 5.2 km.

Further Tests and Discussion of the Inversion Results

The relatively small uncertainty of the depth estimate for the HYPOSAT solution is, of course, a formal error. This error may not represent the real uncertainty of the depth estimate, which must be investigated in more detail. Using the COMB model configuration, we performed several additional location tests.

The first test was to investigate the sensitivity of the COMB location to data from the nearest station AMD. Starting with a trial depth of 0 km, the data were inverted with

different combinations of AMD contributions, (a) without any AMD observations, (b) only with the Pn , or (c) only with the Sn onset, and (d) with both onsets, with or without also inverting the travel-time difference $Sn-Pn$. The result is that only if we include *both* the Pn and the Sn onset times at AMD (in any combination), the depth of the event can be resolved as about 20 km.

Next, we tested how much the estimated source depth for the COMB location depends on the initial depth in the inversion; a set of trial depths of 0, 10, 20, and 30 km were employed with an initial point close to the epicentral area. In all cases, the inversion converged to a depth between 15 and 20 km.

Then, residuals and misfit were calculated for COMB solutions with fixed depths. The fixed depth was systematically changed in 1-km steps between 0 and 40 km. Not surprisingly, the depth range with the minima for the different quality measures (rms, WMF, size of the error ellipse) is rather wide. We assume that all acceptable solutions should not deviate more than +5% from the smallest values found. Then, the best depth range with the smallest rms values is 5–16 km (minimum at 10 km), with the smallest WMF values is 12–27 km (minimum at 21–22 km), and with the smallest size of the error ellipses is 14–22 km (minimum at 18 km). From these results, we can deduce a likely depth in the range 10–22 km.

Finally, the depth estimate may also depend on the V_p/V_s ratio of the models. Since the results of Wadati's method define the V_p/V_s ratio in the uppermost mantle, only a change in the V_p/V_s ratio in the crust might be able to move the depth. We have changed the V_p/V_s ratio in the crust over an extended range from 1.4 to 1.9 and relocated the event. The best locations found were always in the lower crust with increased travel-time residuals for the S -type onsets.

The results for the global models IASP91 and AK135 can be rejected since they cannot model the observed data. Therefore, we can focus on the results with the regional models BAREY, BAREZ, and their combination (COMB). For these models, the locations determined by applying different location techniques agree quite well as shown by some overlap of their confidence regions or error ellipses. From both the shakeNA and the HYPOSAT results we conclude that the event was most likely an earthquake in the middle or lower crust at about 10–30 km depth (see Table 3). Such deep crustal events are often attributed to the long-term effects of ice unloading from the last glaciation, and were previously observed around Novaya Zemlya (e.g., Marshall *et al.*, 1989; Ringdal, 1997).

Additional information provides further support for the interpretation that the 02:11 UT event was not an underwater explosion:

- A spectral analysis of the observed seismic signals does not show any indication of bubble pulse reverberations, which are typical for underwater events and which were observed, for example, for the Kursk submarine accident

- in the Barents Sea (e.g., Koper *et al.*, 2001; Schweitzer, 2002a).
- Bowers (2002) investigated the spatial distribution of seismic energy radiated by this event in the Kara Sea and concluded that it is best fitted with a double-couple radiation from an east–west-striking reverse fault.
 - About four hours after the present event, another event about one magnitude unit smaller in the same epicentral area was recorded at AMD and SPITS (Ringdal *et al.*, 1997); this smaller event can be interpreted as aftershock. Recently, Gibbons and Ringdal (2006) could also identify signals of this aftershock in the array data of the large NORSAR array.

Comparison with Data Center Solutions

The international data centers PIDC (REB), National Earthquake Information Center (NEIC) (PDE), and ISC have also provided location estimates for this event in the Kara Sea. All centers used slightly different observations and reached different locations as listed in Table 4. Figure 7 displays these epicenter estimates (REB: diamond, PDE: hexagon, ISC: dot) with their published error ellipses in black together with our COMB solution (star) for all available data in gray (see Table 3). The number of constraining observations for the ISC location is relatively large because the ISC used in its inversion the data from the arrays SPITS, FINES, and NORES twice: once under the array-beam name and once under the name of the central site of the array (SPA0, FIA0, and NRA0).

The precise travel-time curves, location algorithms, and applied data uncertainties of the data center solutions are unknown to us. Therefore, it is difficult to compare our solutions directly with those provided by the data centers. Be-

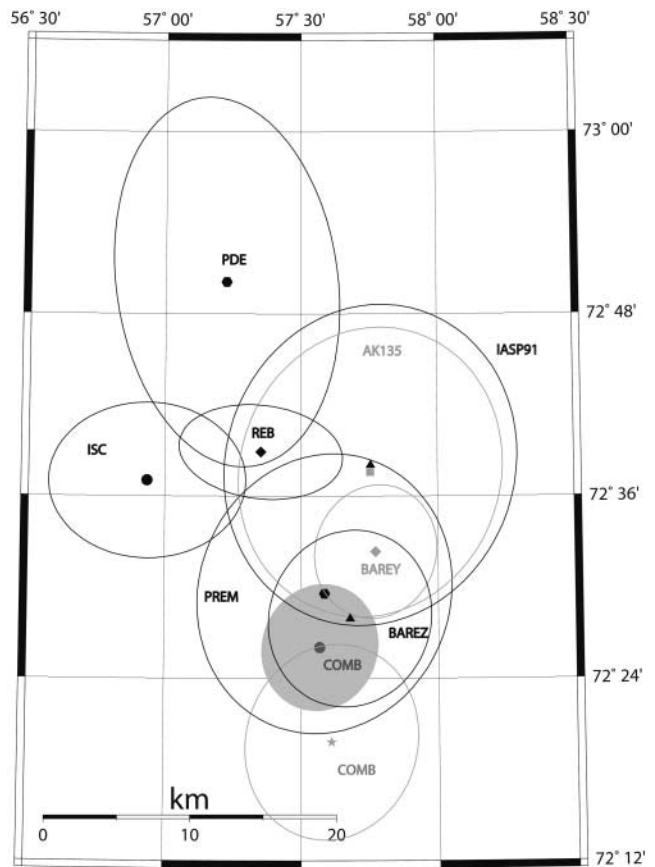


Figure 7. Epicenters and error ellipses for the Kara Sea event of 16 August 1997 as published by data centers, and as estimated by our relocation experiment using only a limited set of data. The error ellipse of the COMB solution for the limited data set is shown as a gray-shaded area. For further details, see text and Table 4.

Table 4

Hypocenter Solutions for the 16 August 1997 Event in the Kara Sea as Published by International Data Centers and the Event Locations Performed for Comparison with Our Results

Model	Latitude (°)	Longitude (°)	<i>D</i> (km)	Time	<i>P</i>	<i>S</i>	BAZ	<i>P</i>	TTD	rms (sec)	WMF	Δ (km)	EE (km ²)
REB	72.648	57.352	0	02:10:59.9	5(5)	0(4)	3(5)	3(5)	0(3)	0.20	1.77	36.5	179
PDE	72.835	57.225	10	02:10:59.77	7(7)	0(3)	0(?)	0(?)	0(3)	1.42	0.93	57.8	963
ISC	72.617	56.935	10	02:10:59.18	13(13)	0(9)	0(?)	0(?)	0(6)	1.30	1.08	39.3	358
JB	72.629	57.749	18	02:10:53.99	10(10)	6(6)	7(7)	6(7)	4(4)	4.16	3.56	33.6	1100
PREM	72.493	57.585	18	02:10:59.65	10(10)	6(6)	7(7)	6(7)	4(4)	3.57	2.76	18.2	830
IASP91	72.634	57.754	18	02:10:56.43	10(10)	6(6)	7(7)	6(7)	4(4)	4.30	3.73	34.3	1095
AK135	72.626	57.754	18	02:10:56.84	10(10)	6(6)	7(7)	6(7)	4(4)	3.88	3.34	33.4	891
BAREY	72.549	57.772	18	02:11:02.57	10(10)	6(6)	7(7)	7(7)	4(4)	1.35	1.23	23.9	190
BAREZ	72.466	57.678	18	02:11:03.98	9(10)	4(6)	4(7)	1(7)	2(4)	2.39	1.70	15.3	337
COMB	72.434	57.568	18	02:11:03.08	10(10)	6(6)	7(7)	7(7)	4(4)	1.36	0.85	11.7	171

Listed are the source parameters including their fixed depth *D* and the number of input data used in the location (*P*- and *S*-onset times, backazimuth values [BAZ], ray parameters [*P*], and travel-time differences [TTD]). The maximum possible number for each input data type is shown in parentheses; note such values are not available for NEIC and ISC. rms is calculated from the constraining onset times, WMF is the weighted misfit for all possible travel-time observations (in the case of data center solutions for all onsets, for which residuals were published), and Δ gives the epicentral distance between this solution and the COMB solution of Table 3. EE lists the size of the error ellipse as plotted in Figure 7. For further details, see text.

cause we could invert much more data than the data centers, an open question is if the data centers could reach a solution similar to our best result (COMB, see Fig. 5 and Table 3; also shown on the map in Fig. 7 as star) with their limited set of available data.

To investigate this problem, we selected just those readings from stations listed in the ISC bulletin (all entries marked with a “C” in Table 2). This subset of the data cannot provide any depth resolution because it does not contain readings from station AMD. Therefore, we have employed a fixed depth of 18 km (taken from the COMB solution for the whole data set; see Table 3) for all the following inversions.

We relocated the event with HYPOSAT for a set of different standard Earth models. The results are also listed in Table 4 and shown on the map in Figure 7: JB (Jeffreys and Bullen, 1940), PREM (Dziewonski and Anderson, 1981, black, hexagon), IASP91 (Kennett and Engdahl, 1991, black, triangle), and AK135 (Kennett *et al.*, 1995, gray, square) and for the three models derived for the Barents Sea region (BAREY [gray, diamond], BAREZ [black, triangle], and COMB [dot, with error ellipse as gray-shaded area]). Model COMB is again the combined usage of BAREY and BAREZ for specific paths (see Table 1). The result for the model JB is not shown on the map because it is too similar to the IASP91 solution.

In Table 4, we present the number of constraining input data used for the locations, the rms values of all onset times employed in the location, and the epicentral distance to our best solution (COMB, see Fig. 5 and Table 3). WMF values are calculated for each of the solutions. For the data center solutions, we used the data uncertainties as given in Table 2, but the residuals as published in the bulletins. Note that in the REB and in the ISC bulletin an S_n reading from station ARU is listed, but was not used to locate the event; this onset with a residual of -20.8 sec was ignored when the WMF value for the REB solution was calculated.

The relocations for the three global models JB, IASP91, and AK135 are very close to each other and from the data center solutions, only the REB solution lies within the larger error ellipses from our relocations. The relatively small error ellipse of the REB solution is mainly caused by the fact that the S_n onsets with their large residuals were not used as constraining data for the solution. In our relocations, all onsets were used and contribute with their residuals to the larger error ellipses. In all these solutions, the P -type onsets are more or less equally well explained but the S_n onsets are not. Because this could arise from a depth effect, we also relocated the event with fixed depths of 0 km and 10 km. For all four global models (JB, PREM, IASP91, and AK135) the residuals were smallest with a fixed depth of 18 km.

The smallest residuals from our inversions were obtained for the new regional models (see the locations on the map in Fig. 7). The most uncertain of these solutions is for model BAREZ, which explains well the readings from stations in the western Barents Sea, at AMD, and at NRIS. The

subset of data, used in this experiment, contains such readings only from the SPITS array. All other readings are from Fennoscandia or the Kola Peninsula. For these data, model BAREY gives in the mean a better representation of the S_n -onset times. Consequently, the location with model BAREY has smaller residuals. However, the 90% confidence error ellipse of the barez solution contains the solutions for the models BAREY and COMB and overlaps with the error ellipse of our best solution COMB.

Again, the residuals show a non-Gaussian distribution (Fig. 8). For comparison, the distribution of the travel-time residuals of the COMB solution for all data is plotted again in the right lower corner. The residuals and the error ellipse for model COMB are the smallest and this solution is the closest to our COMB solution for the full data set—the positive effect of using path-specific velocity models.

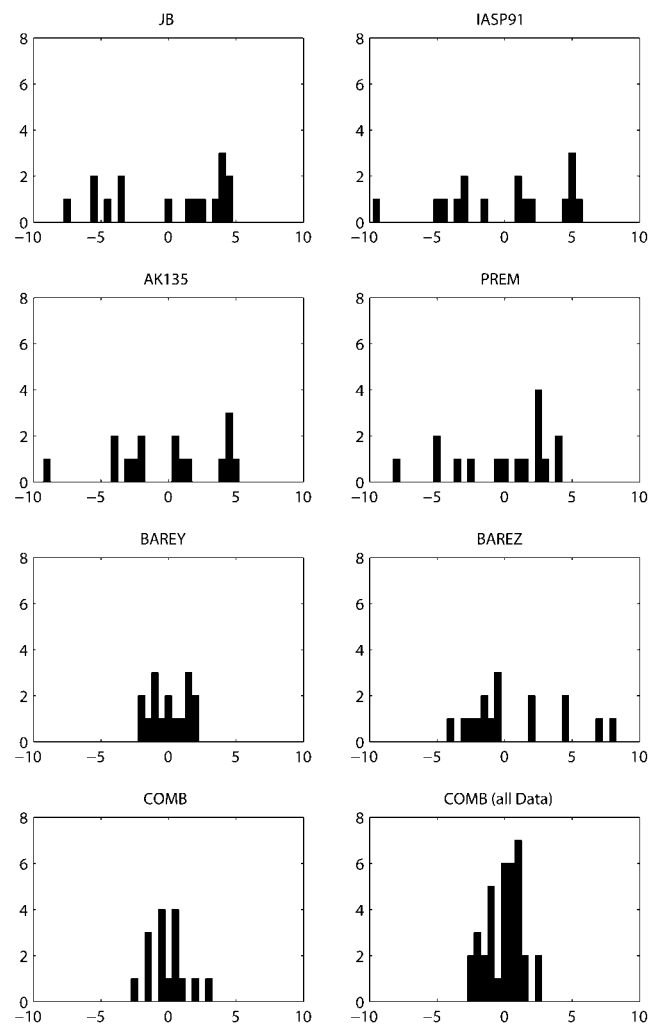


Figure 8. Histogram of all travel-time residuals in seconds for the HYPOSAT locations in Figure 7, achieved by utilizing the reduced data set for evaluation of the data center locations.

Conclusions

This study has confirmed both the importance of *S*-wave information in assessing the depth of regional events, and the need to get a good regional velocity model for both *P* and *S* to place the strongest constraints on the location of the event. Then, as the comparison with the data center solutions showed, the presumable area, in which the epicenter has to be searched, can be determined even with a more limited set of observations.

The comparisons of the different data center solutions with our own inversions indicate that using only a limited data set, but an adequate travel-time model, it is possible to locate the epicenter of the event in the Kara Sea relatively close to our best COMB location. However, the depth resolution of such limited data sets is of course negligible. The relative small error ellipses of the published solutions are a problem, which arises when using only a limited number of data; then the corresponding data and modeling errors can bias the solution toward one direction. The size of an error ellipse is directly related to the importance of each single-input datum for the solution and the *a posteriori* residuals. A solution of a limited data set may explain the observations in a heterogeneous structure quite well but may be far away from the real hypocenter. With the usually made assumption that the reading errors and the *a posteriori* residuals have an unbiased normal distribution, such inversion results may presume an apparently high resolution and accuracy of the solution.

The location estimates for the whole data set from the different location techniques agree quite well, with some overlap of the estimated confidence regions. The event occurred most likely in the middle or lower crust between 10 and 30 km depth.

Acknowledgments

The research presented was supported in part by the Defense Threat Reduction Agency and monitored by AFTAC, Patrick AFB, Florida 32925, under contract no. F08650-01-C-0055, and in part by the Norwegian Research Council, which supported a visit by B.L.N. Kennett to NORSAR through a Senior Scientist Fellowship. We thank all station operators at the Universities of Bergen and Helsinki, the PIDC, GEOFON, IRIS, and the Kola Science Center for providing us with additional data from the Norwegian seismic network, the Finnish seismic network, the Apatity array, and the three-component seismic stations AMD, ARU, KBS, KEV, and NRIS. We acknowledge critical reviews of the manuscript by D. Bowers, J. Pujol, and an anonymous reviewer. All maps were plotted using the GMT software package (Wessel and Smith, 1995). This article is NORSAR Contribution Number 850.

References

Akaike, H. (1974). Markovian representation of stochastic processes and its application to the analysis of autoregressive moving average processes, *Ann. Inst. Statist. Math.* **26**, 363–387.

Billings, S., M. S. Sambridge, and B.L.N. Kennett (1994). Errors in hypo-

center location: picking, model and magnitude dependence, *Bull. Seism. Soc. Am.* **84**, 1978–1990.

Bowers, D. (2002). Was the 16 August 1997 seismic disturbance near Novaya Zemlya an earthquake? *Bull. Seism. Soc. Am.* **92**, 2400–2409.

Buland, R., and C. H. Chapman (1983). The computation of seismic travel times, *Bull. Seism. Soc. Am.* **78**, 780–798.

Bungum, H., O. Ritzmann, N. Maercklin, J. I. Faleide, W. D. Mooney, and S. T. Detweiler (2005). Three-dimensional model for the crust and upper mantle in the Barents Sea region, *EOS Trans. AGU* **86**, 160–161.

Dziewonski, A. M., and D. L. Anderson (1981). Preliminary reference Earth model, *Phys. Earth Planet. Interiors* **25**, 297–356.

Gibbons, S. J., and F. Ringdal (2006). The detection of low magnitude seismic events using array-based waveform correlation, *Geophys. J. Int.* **165**, 149–166, doi 10.1111/j.1365-246X.2006.02865.x

GSE/Japan/40 (1992). A fully automated method for determining the arrival times of seismic waves and its application to an on-line processing system, Presented at Proceedings 34th GSE Session, Geneva, Switzerland.

Hartse, H. E. (1998). The 16 August 1997 Novaya Zemlya seismic event as viewed from GSN stations KEV and KBS, *Seism. Res. Lett.* **69**, 206–215.

Hicks, E. C., T. Kværna, S. Mykkeltveit, J. Schweitzer, and F. Ringdal (2004). Travel-times and attenuation relations for regional phases in the Barents Sea region, *Pure Appl. Geophys.* **161**, 1–19.

Jeffreys, H., and K. E. Bullen (1940). *Seismological Tables*, British Association for the Advancement of Science, London, 50 pp.

Kennett, B.L.N. (2004). Consistency regions in non-linear inversion, *Geophys. J. Int.* **157**, 583–588.

Kennett, B.L.N., and E. R. Engdahl (1991). Travel times for global earthquake location and phase identification, *Geophys. J. Int.* **105**, 429–466.

Kennett, B.L.N., E. R. Engdahl, and R. Buland (1995). Constraints on seismic velocities in the Earth from traveltimes, *Geophys. J. Int.* **122**, 108–124.

Koper, K. D., T. C. Wallace, St. R. Taylor, and H. E. Hartse (2001). Forensic seismology and the sinking of the Kursk, *EOS Trans. AGU* **82**, 37, 45–46.

Kremenetskaya, E., V. Asming, and F. Ringdal (2001). Seismic location calibration of the European Arctic, *Pure Appl. Geophys.* **158**, 117–128.

Kværna, T. (1995). Automatic onset time estimation based on autoregressive processing, Semiannual Technical Summary I April–30 September 1995, NORSAR Sci. Rep. 1-95/96, 113–133.

Levshin, A. L., M. H. Ritzwoller, M. P. Barmin, A. Villasenor, and C. A. Padgett (2001). New constraints on the arctic crust and uppermost mantle: surface wave group velocities, Pn and Sn, *Phys. Earth. Planet. Interiors* **123**, 185–204.

Marshall, P. D., R. C. Stewart, and R. C. Lilwall (1989). The seismic disturbance on 1986 August 1 near Novaya Zemlya: a source of concern? *Geophys. J. Int.* **98**, 565–573.

Menke, W. (1989). *Geophysical Data Analysis: Discrete Inverse Theory, Revised Ed., International Geophysics Series 45*, Academic Press, San Diego, xii + 289 pp.

Mooney, W. D., G. Laske, and T. G. Masters (1998). CRUST 5.1: a global crustal model at $5^\circ \times 5^\circ$, *J. Geophys. Res.* **103**, 727–747.

Mykkeltveit, S., and F. Ringdal (1981). Phase Identification and event location at regional distance using small-aperture array data, in *Identification of Seismic Sources: Earthquake or Underground Explosion*, E. S. Husebye and S. Mykkeltveit (Editors), NATO Advanced Study Institute Series, Dordrecht, The Netherlands, 467–481.

Press, W. H., S. A. Teukolsky, W. T. Vetterling, and B. P. Flannery (1992). *Numerical recipes in FORTRAN, the art of scientific computing, Second Ed.*, Cambridge University Press, Cambridge.

Ringdal, F. (1997). Study of low-magnitude seismic events near the Novaya Zemlya nuclear test site, *Bull. Seism. Soc. Am.* **87**, no. 6, 1563–1575.

Ringdal, F., T. Kværna, E. O. Kremenetskaya, and V. E. Asming (1997). The seismic event near Novaya Zemlya on 16 August 1997, NORSAR

- Semiannual Technical Summary 1 April–30 September 1996, NORSAR Sci. Rep. 1-97/98, 110–119.
- Sambridge, M. S., and B.L.N. Kennett (2001). Seismic event location: Non-linear inversion using a neighbourhood algorithm, *Pure Appl. Geophys.* **158**, 241–257.
- Schweitzer, J. (2001). HYPOSAT: an enhanced routine to locate seismic events, *Pure Appl. Geophys.* **158**, 277–289.
- Schweitzer, J. (2002a). Some results derived from the seismic signals of the accident of the Russian submarine Kursk, NORSAR Semiannual Technical Summary 1 July–31 December 2002, NORSAR Sci. Rep. 1-2002, 115–121.
- Schweitzer, J. (2002b). PD 11.1: User manual for HYPOSAT (including HYPOMOD), in *IASPEI New Manual of Seismological Observatory Practice (NMSOP)*, Vol. 2, P. Bormann (Editor), GeoForschungs-Zentrum, Potsdam, 16 pp.
- Wadati, K. (1933). On the travel time of earthquake waves, Part II, *Geophys. Mag. (Tokyo)* **7**, 101–111.
- Wessel, P., and W.H.F. Smith (1995). New version of Generic Mapping Tools released, *EOS Trans. AGU* **76**, 329.
- NORSAR
PO Box 53
N-2027 Kjeller, Norway
johannes.schweitzer@norsar.no
(J.S.)
- Research School of Earth Sciences
The Australian National University
Canberra, ACT 0200, Australia
Brian.Kennett@anu.edu.au
(B.L.N.K.)

Manuscript received 19 February 2004.